

Article

Experimental Investigation on Relations Between Impact Resistance and Tensile Properties of Cement-Based Materials Reinforced by Polyvinyl Alcohol Fibers

Ju Zhang ^{1,2}, Pucun Bai ^{1,*}, Changwang Yan ^{2,*}, Shuguang Liu ^{1,2} and Xiaoxiao Wang ¹

¹ School of Materials Science and Engineering, Inner Mongolia University of Technology, Hohhot 010051, China; zj970741@126.com (J.Z.); liusg6011@126.com (S.L.); wxiaoxiao.good@163.com (X.W.)

² School of Mining and Technology, Inner Mongolia University of Technology, Hohhot 010051, China

* Correspondence: pcbai@imut.edu.cn (P.B.); yanchangwang@imut.edu.cn (C.Y.); Tel.: +86-139-4881-0199 (P.B.); +86-152-4717-9956 (C.Y.)

Received: 27 September 2019; Accepted: 17 October 2019; Published: 18 October 2019



Abstract: Cement-based material is brittle and is easily damaged by an impact load with a few blows. The purpose of this paper is to study the relations between the impact resistance and tensile properties of cement-based materials reinforced by polyvinyl alcohol fiber (PVA-FRCM). A drop-weight test and uniaxial tension test were performed. The relations were studied based on the experimental results, including the relation between the blow number and the tensile stress at the first visible cracking (σ_c) and the relation between the blow number and the tensile strain at the ultimate failure (ε_f). Results showed that the blow number for the first visible crack for disc impact specimens increases obviously with the increase of σ_c of slab specimens. The crater diameter and blow number for ultimate failure of the disc specimens increase with the increase of ε_f of slab specimens. For the PVA-FRCM specimens with larger σ_c and ε_f , much more blows are needed to cause both the first visible crack and ultimate failure. Polyvinyl alcohol fibers can reinforce impact resistance and tensile properties of cement-based materials.

Keywords: PVA-FRCM; drop-weight test; uniaxial tension test; stress for the first visible crack moment; strain for the failure moment

1. Introduction

Cement-based material, such as concrete, is brittle and is easily damaged by impact load with a few blows [1,2]. Thus, various fibers, e.g. steel fiber, polypropylene fiber, and carbon fiber, are added into the mixture to improve its impact resistance. The effects of the cellulose, polypropylene, and steel fibers on the impact resistance of the cement-based material were studied by Rahmani [3], among which the effect of steel fiber was the most significant. The mean failure blows were increased from 48 to 228 after steel fibers were added. Nataraja et al. [4] conducted the drop-weight test on steel fiber-reinforced concrete. It was known from the test that the failure blows increased with the increase of the steel fiber volume content. The impact resistance of the concrete with steel fiber volume content of 1.5% was about 20–25 times to the one of its plain counterpart. Wang et al. [5,6] used the steel fibers to improve the impact resistance of light weight aggregate concrete. The mean failure blows were increased by 13 times when the steel fiber volume content was 2%. Mastali et al. [7,8] reinforced the self-compacting concrete with the regenerated carbon fiber and the recycled glass fiber. The impact resistance increased 6.48 times for the cylinder specimens with regenerated carbon fiber content of 1.25% and 6.14 times for the ones with regenerated glass fiber volume content of 1.25%.

These research results states clearly that the impact resistance of concrete can be improved after fibers are introduced into the specimen. This is possibly attributed to that the fibers can improve the tensile toughness of concrete [9]. When the fiber-reinforced concrete fails under the tensile load, it reached a large strain [10,11]. So much more blows are needed for the fiber-reinforced concrete under the impact load.

Cement-based material reinforced by polyvinyl alcohol fiber (PVA-FRCM) is tough [12] and its ultimate strain can exceed 3% under uniaxial tensile load. Its extreme tensile strain capacity is hundreds of times larger than the one of plain concrete. Li et al. [13,14] conducted the uniaxial tension test to measure the stress versus strain curves of PVA-FRCM. Results showed that the tensile strain capacity exceeded 4%. The same strain level of PVA-FRCM was realized by Nematollahi et al. [15] and Li et al. [16]. Due to the higher tensile deformation capacity, the impact resistance performance of PVA-FRCM was better. Yang et al [17] reported a drop-weight tower test on a PVA-FRCM square-shaped panel. The results showed that a longer segment of plastic yielding appeared. The generation of cracks was delayed, and the surface of panel exhibited multiple micro-cracks under the quasi-static load. Toutanji et al. [18,19] conducted the Charpy U-notch test to assess the impact energy absorption capacity of PVA-FRCM. It was found that the absorbed energy increased when the PVA fibers were added to 0.9% volume content, and then it started to decrease when the fiber volume content reached from 0.9% to 1.2%. Mechtcherine et al. [20,21] analyzed the impact behavior of PVA-FRCM by the Hopkinson bar test method. Due to the large amount of micro-cracks, its impact energy absorption capacity was higher. Atahan et al. [22] employed Charpy impact experiments to study the influences of fiber volume content on the impact energy absorption capacity of PVA-FRCM. Compared with the plain ones, when the polyvinyl alcohol (PVA) fiber volume content reached 0.5%, 1.0%, 1.5%, and 2.0%, the absorbed impact energy was increased by 7%, 8%, 11%, and 36%, respectively.

The literature introduced above shows that fibers can improve the impact resistance of concrete. Especially PVA-FRCM, its impact energy absorption capacity is higher due to its multiple micro-cracks characteristics. However, for the current state of knowledge, although there are already interesting and constructive results about PVA-FRCM involving material design [23,24], mechanical investigations [25, 26], durability [27,28], and applications [29,30], to the best of our knowledge, no studies have been conducted to show the relationships between the impact resistance and multiple micro-cracks induced by tensile load. Therefore, the purpose of this paper is to evaluate relations between the impact resistance and tensile properties of PVA-FRCM. To this scope, the drop-weight test and the uniaxial tension test were performed, the test results were analyzed and the relationships between the blow numbers and tensile properties were evaluated.

2. Experimental Program

2.1. Materials

Components of the PVA-FRCM in this study contain the PVA fiber, cement, fly ash, quartz sand, hydroxyl-propyl methyl cellulose (HPMC) and superplasticizer. In the PVA-FRCM mixture, the type of PVA fiber is KII-REC15. The properties of the PVA fiber are shown in Table 1. Portland cement with a model of P.O 42.5R was produced in Hohhot. The chemical composition of cement is presented in Table 2. Class I fly ash from the power station in Erdos was adopted and its chemical composition is listed in Table 3. Quartz sand originated from Tongliao was adopted. The sand size was from 0.075 mm to 0.106 mm. HPMC was produced in Jinan. 3301E superplasticizer was produced in Dalian.

Table 1. Properties of polyvinyl alcohol (PVA) fiber.

Type	Diameter (mm)	Length (mm)	Nominal Strength (MPa)	Elongation (%)	Young's Modulus (GPa)	Density (g/cm ³)
KII-REC15	0.04	12	1600	6	40	1.3

Table 2. Chemical composition of cement.

Index	Al ₂ O ₃	SiO ₂	CaO	Fe ₂ O ₃	MgO	SO ₃	Loss on Ignition
Content (%)	7.19	23.44	55.01	2.96	2.24	2.87	2.86

Table 3. Chemical composition of class I fly ash (%).

SiO ₂	Al ₂ O ₃	CaO	Fe ₂ O ₃	CO ₂	MgO	SO ₃	K ₂ O	Na ₂ O	TiO ₂	SrO	Others
40.28	18.15	18.08	8.56	5.18	2.34	2.08	1.76	1.31	0.95	0.73	0.58

The mixture proportion of PVA-FRCM is shown in Table 4. The water–binder ratio of the mixture was fixed at 0.26 throughout the test. In the mixture proportion, PVA fiber volume contents (V_f) were 0, 0.5%, 1.0%, 1.5%, and 2.0%. The specimens were named in F0, F0.5, F1, F1.5, and F2 to represent the above PVA fiber volume contents respectively. HPMC and superplasticizer were added into the mixture at a cement weight of 0.05% and 2% respectively.

Table 4. Mixture proportions of cement-based material reinforced by polyvinyl alcohol fiber (PVA-FRCM) (kg/m³).

Material	Cement	Fly Ash	Water	Quartz Sand	HPMC	Superplasticizer
PVA-FRCM	943	283	245	566	0.27	18.87

2.2. Specimen Preparation

When the specimens prepared, the cement, fly ash and quartz sand in a dry state were mixed firstly in a 100-liter mixer with rotating blade for two minutes. Then the 80% of the water and the superplasticizer were added into the mixture. The remaining water and the HPMC were added after 2 min of mixing. After mixed for another one minute, the PVA fibers were added manually and gradually for ensuring the most random dispersion in the cementitious matrix. Then all ingredients were continuously mixed for five minutes before the mixture was poured into the mold.

There were two types of specimens in this test. One type of specimen was for the uniaxial tension. This type of specimen had a shape of dumbbell. For the test section of the specimen, it was just a rectangular slab. Its length was 90 mm, width was 30 mm and thickness was 15 mm. The other type of specimen was for the drop-weight test and it had a shape of disc. Its diameter was 152 mm and its thickness was 63.5 mm. For the first type, three specimens were prepared for each V_f . Six specimens were prepared for each V_f of the second type. The average cubic compressive strength of PVA-FRCM was about 50 MPa at the age of 28 days.

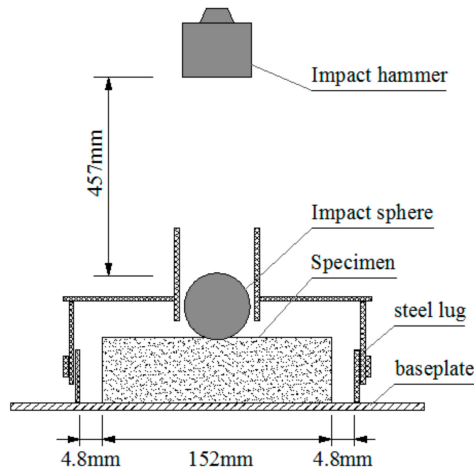
All the specimens were kept in the laboratory for 24 hours and were cured in the natural water with a room temperature of 24 ± 3 °C for 28 days after demolding. After curing, all the specimens were stored indoor for another 28 days with a room temperature of 24 ± 3 °C and a relative humidity of 85 ± 10 %. Taking into account the use of fly ash, to minimize the effects of fly ash on the early-age properties of PVA-FRCM such as modulus of elasticity or early-age shrinkage, both drop-weight and uniaxial tension tests were conducted at age of 56 days of the specimens in this study.

2.3. Test Methods

2.3.1. Drop-Weight Test

The drop-weight test apparatus was designed according to the recommendation of American Concrete Institute (ACI)Committee 544 [19], as shown in Figure 1. The 64mm diameter impact sphere was placed on the top of the centre of the disc specimen. The PVA-FRCM disc was collided repeatedly by the impact hammer dropping through the impact sphere. The impact hammer weights 4.54 kg. The distance was 457 mm from the bottom of impact hammer to the top of impact sphere.

The impact test operation was continuous until the disc specimen touched three of the four steel lugs. The blow numbers for the first visible crack (N_c) and for the ultimate failure (N_f) were recorded during the test. The failure pattern and impact crater diameter of PVA-FRCM disc specimen were identified.



(a) Schematic diagram of drop-weight device

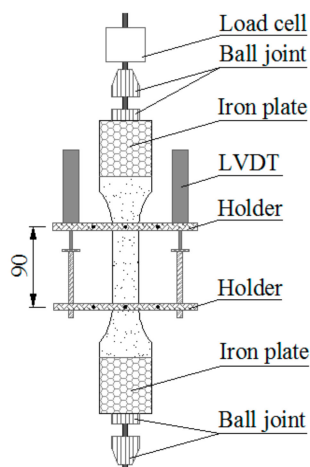


(b) Self-improved equipment for drop-weight test

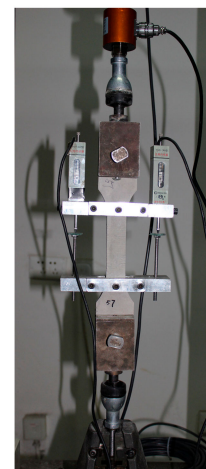
Figure 1. Drop-weight test apparatus with the cement-based material reinforced by polyvinyl alcohol fiber PVA-FRCM disc.

2.3.2. Uniaxial Tension Test

The uniaxial tension test was accomplished on the universal testing machine. Loading apparatus are shown in Figure 2. Two iron plates were fixed to both ends of the slab specimen by epoxy. In order to ensure the uniaxial tension, two ball joints were connected to the iron plates at the ends of the specimen. The loading rate was 0.1 mm/min and kept constant from the beginning. The tensile load was measured by a load cell. The tensile deformation was measured by linear variable differential transformers (LVDTs). The data acquisition system was used to acquire the load and deformation values simultaneously. The crack patterns of specimen were captured into pictures.



(a) Schematic diagram of loading device for tension test



(b) Loading apparatus for tension test

Figure 2. Specimen and loading apparatus for tension test.

3. Drop-Weight Test Results and Analysis

3.1. Failure Patterns

Figure 3 shows the failure patterns of PVA-FRCM disc specimens with different V_f . Subjected to impact hammer dropping repeatedly, disc specimens were broken into three or four pieces. The orientations of cracks have a common origin at the center of crater and exhibited about 90 degrees, 120 degrees and 180 degrees angle between each other. The disc specimens containing more PVA fibers, e.g. F1.5 and F2, failed with more debris and their fibers were pulled out, while the PVA fibers were snapped for the specimens with less PVA fibers.

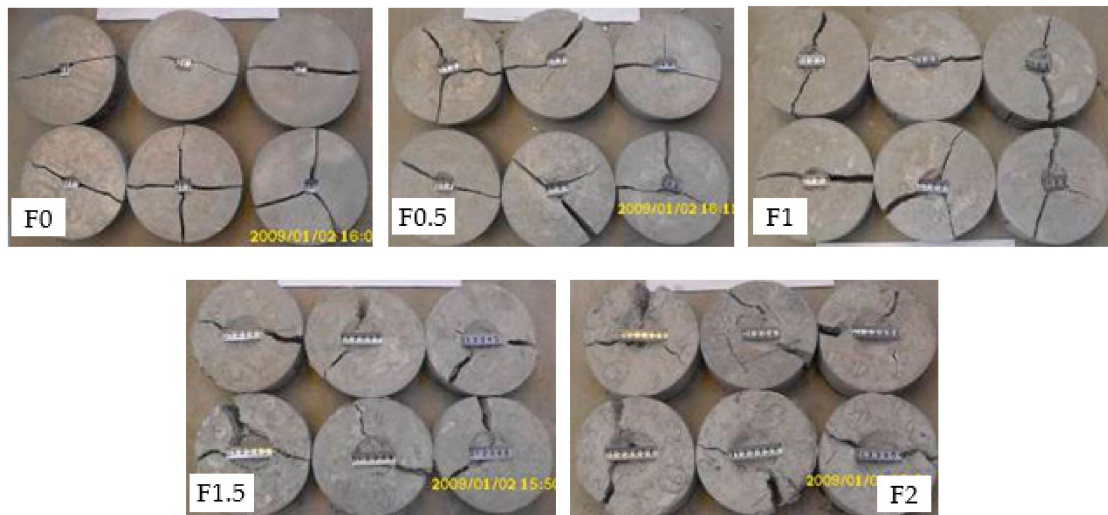


Figure 3. Failure patterns of PVA-FRCM disc specimens.

The impact craters were observed in the center of disc specimens when the disc specimen failed, as shown in Figure 4. The specimen F0 had the smallest impact crater diameter. The specimen F2 had the biggest impact crater diameter of 59 mm that was nearly the same size of the diameter of the impact sphere.



Figure 4. Impact craters of PVA-FRCM disc specimens.

The diameters of impact craters for all specimens are listed in Table 5. The relationship between V_f and average diameter of impact crater is shown in Figure 5. The confidence level is 95%, and uncertainty of the test methods ranges from 2.0 to 4.8. It is found from the histogram that as the V_f increases the diameter of the impact crater becomes larger and larger. This phenomenon indicates that the energy consumed by the specimen during dropping repeatedly would become more, when more PVA fibers are added into the disc specimen.

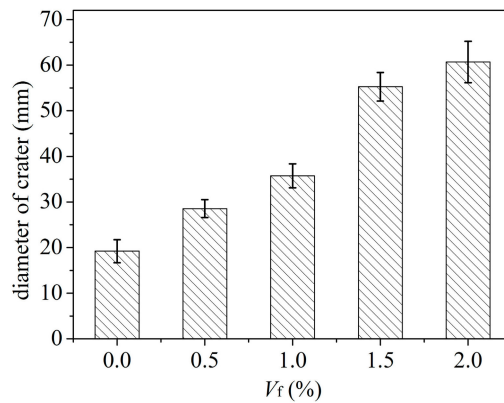


Figure 5. Influence of PVA fiber volume contents (V_f) on diameter of impact craters.

Table 5. Test results of PVA-FRCM under drop weight impact load.

No.	V_f (%)	Diameter of Crater (mm)	N_c	N_f	$\Delta = N_f - N_c$	W_1 (J)	W_2 (J)
1	0	16.7	1	2	1	20.33	40.67
2	0	20.2	1	2	1	20.33	40.67
3	0	17.8	2	4	2	40.67	81.33
4	0	21.1	1	2	1	20.33	40.67
5	0	22.8	1	2	1	20.33	40.67
6	0	16.7	2	5	3	40.67	101.66
average		18.95	1	2	1	27.11	57.61
1	0.5	28.1	3	18	15	61.00	365.99
2	0.5	27.4	33	58	25	670.98	1179.30
3	0.5	30.6	15	42	27	304.99	853.98
4	0.5	25.8	3	12	9	61.00	243.99
5	0.5	31.0	5	22	17	101.66	447.32
6	0.5	28.4	20	47	27	406.66	955.64
average		29.53	11	32	21	267.72	674.37
1	1.0	34.8	160	370	210	3253.26	7523.15
2	1.0	35.2	155	245	90	3151.59	4981.55
3	1.0	36.3	32	255	223	650.65	5184.88
4	1.0	32.1	36	109	73	731.98	2216.28
5	1.0	40.2	128	236	108	2602.60	4798.55
6	1.0	35.7	11	39	28	223.66	792.98
average		35.95	88	211	123	1768.96	4249.56
1	1.5	52.8	437	975	538	8885.45	19824.52
2	1.5	52.6	543	1133	590	11040.73	23037.11
3	1.5	53.4	200	1710	1510	4066.57	34769.16
4	1.5	60.6	590	1857	1267	11996.38	37758.09
5	1.5	54.9	1712	2538	826	34809.83	51604.76
6	1.5	57.2	1650	2370	720	33549.19	48188.84
average		55.8	805	1584	779	17391.36	35863.75
1	2.0	63.5	215	2261	2046	4371.56	45972.56
2	2.0	51.8	750	2226	1476	15249.63	45260.91
3	2.0	61.2	1394	3251	1857	28343.98	66102.08
4	2.0	63.5	2603	3727	1124	52926.39	75780.51
5	2.0	63.5	2782	4084	1302	56565.97	83039.33
6	2.0	60.6	1900	2866	966	38632.40	58273.93
average		59.28	1662	3018	1456	32681.66	62404.89

Note: N_c and N_f are the blow numbers for the first visible crack and ultimate failure; W_1 and W_2 are the impact energies for the first visible crack and ultimate failure.

3.2. Blow Numbers

The blow numbers for the first visible crack (N_c) and ultimate failure (N_f) of PVA-FRCM disc specimens are listed in Table 5. Because the specimen F0 had no PV fiber added, its average values of N_c and N_f were only one and two respectively. It is evident that the disc specimen without PVA fiber is very brittle and its impact resistance is almost negligible. When the specimens are properly reinforced with PVA fibers, the average values of N_c and N_f increase dramatically. For disc specimens with V_f of 2%, the average values of N_c and N_f reached 1662 and 3018, which appeared good toughness performance.

The effect of V_f on the blow numbers is shown in Figure 6. When the confidence level is 95%, uncertainty of N_c is no more than 320, one of N_f do not exceed 270 and one of $N_f - N_c$ is within 370. It can be found that N_c and N_f of disc specimens increased evidently with the increase of V_f . Especially for the specimens with V_f of more than 1%, the increases of N_c and N_f became remarkable. The conclusion can be drawn that the addition of PVA fibers can improve the impact resistance of cementitious materials.

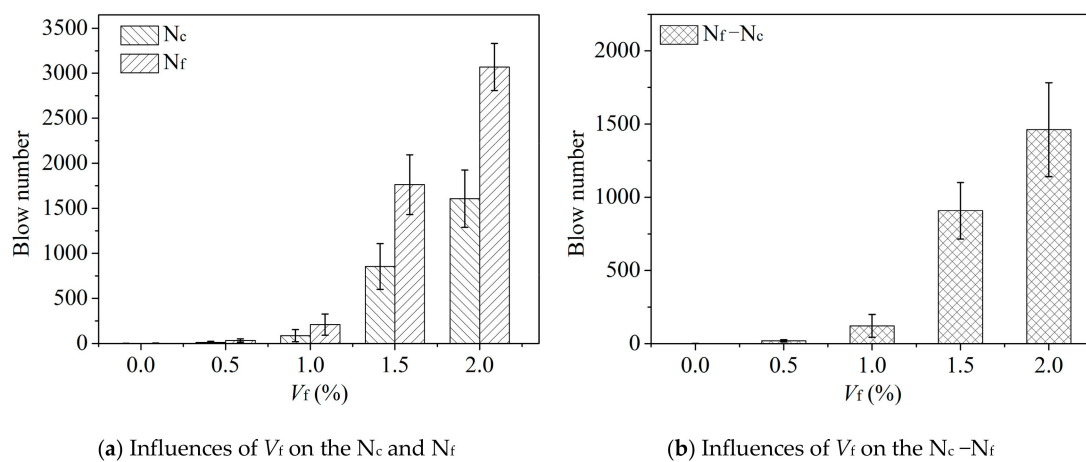


Figure 6. Influences of V_f on blow numbers.

Besides, the difference Δ between N_c and N_f increased simultaneously with the increase of V_f . It increased from 1 to 21, 123, 779, and to 1456 finally, while V_f increased from 0 to 0.5%, 1%, 1.5%, and 2%. This indicates that V_f has a strong influence on the blow number difference between N_c and N_f of the PVA-FRCM disc specimens.

3.3. Impact Energy

The impact energies for the first visible crack and ultimate failure of the disc specimens under the impact load were calculated by the Equation (1) and (2) respectively.

$$W_1 = N_c mgh \tag{1}$$

$$W_2 = N_f mgh \tag{2}$$

where, W_1 and W_2 are the impact energies for the first visible crack and ultimate failure respectively, m is the mass of the impact hammer (4.54 kg), g is the gravitational acceleration (9.8 m/s²), h is the falling distance of the impact hammer (457 mm), and the impact energy is in the unit of joules (J).

The impact energy W_1 and W_2 were calculated and summarized in Table 5. The influence of V_f on the average impact energy are shown in Figure 7. It can be observed that the impact energy for all PVA-FRCM disc specimens increased with V_f . The impact energy had a small increase when V_f is less than 1%, while it had a remarkable increase when V_f is more than 1%. According to the overall tendency, the impact energy at the ultimate failure increases faster with the increase of V_f than the one

at the first visible crack. This indicates that V_f has larger effect on the impact energy at the failure than the one at the first cracking.

These above results regarding the failure patterns, blow numbers, and impact energy of PVA-FRCM were similar to the previous research results [3–8,12–22] which states clearly that the impact resistance of concrete can be improved after fibers (steel, carbon, and PVA fibers) are introduced into the specimen.

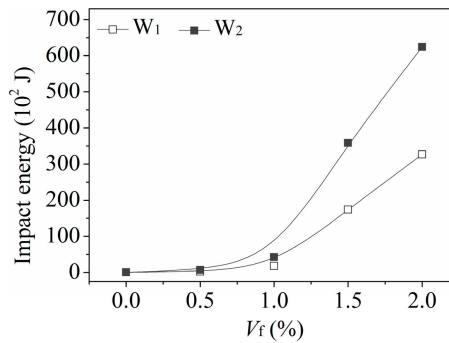


Figure 7. Influence of V_f on impact energy.

4. Uniaxial Tension Test Results and Analysis

This study examined the uniaxial tension test results on the slab specimens, e.g. crack pattern, stress–strain curve, stress and strain at the first visible crack moment (σ_c and ϵ_c), and stress and strain at the failure moment (σ_f and ϵ_f). For the specimen F0, a brittle failure happened under uniaxial tension because no PVA fibers were added. Its stress and strain were so small that they could hardly be captured.

4.1. Crack Pattern under Uniaxial Tension

The crack patterns of the specimens except specimen F0 under uniaxial tension are shown in Figure 8. It can be seen clearly that crack numbers were different for the specimens with different V_f . For the specimen F0.5, only one crack appeared during uniaxial tension test. The first visible crack was exactly the failure crack. When more PVA fibers were added into the specimen, the crack numbers became more. Especially when V_f reached 2%, lots of visible cracks appeared on the surface of the specimen uniaxial tension. The crack numbers of the specimen F1 and F1.5 were in between. It is indicated that V_f has an influence on the crack pattern of the specimens under uniaxial tension.

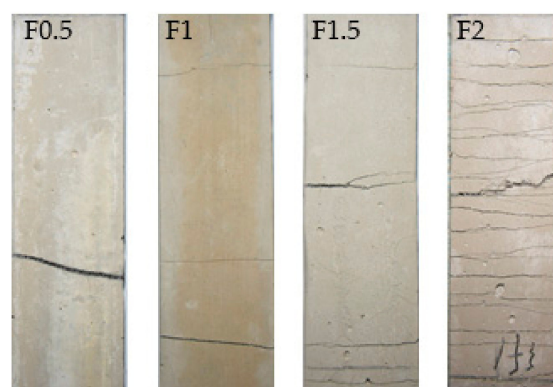


Figure 8. Crack pattern under uniaxial tension.

4.2. Stress–Strain Curves under Uniaxial Tension

The stress–strain curves of all specimens except for the specimen F0 under uniaxial tension are shown in Figure 9. All stress–strain curves contained many small curve segments. A gradual ascending

followed by a sudden descending existed in every small curve segment. Only two curve segments appeared in the stress–strain curves of the specimen F0.5 and F1, while five for the specimen F1.5 and twenty for the specimen F2. The specimens with more PVA fibers had more curve segments. Comparing the number of curve segments in Figure 9 with the number of cracks in Figure 8, it can be found that they were approximately equal. The main reason is probably that the PVA fibers were actually pulled out gradually under uniaxial tension, rather than all PVA fibers being pulled out of the cement matrix simultaneously. When some of the PVA fibers were pulled by the tension transferred by the cement mix, the stress–strain curves exhibited the ascend gradually. Just after these PVA fibers were pulled out, the stress–strain curves exhibited the descend suddenly.

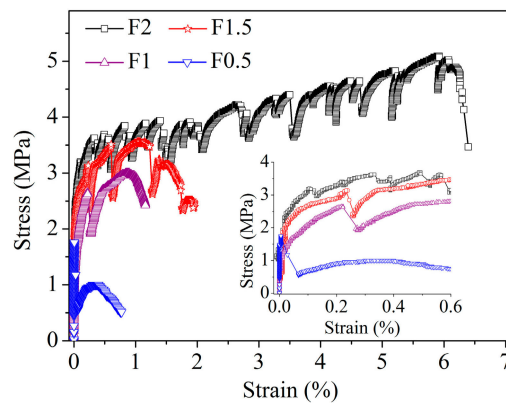


Figure 9. Stress–strain curves under uniaxial tension.

4.3. Influence of V_f on Strain and Stress

All specimens with PVA fibers showed a good toughness performance. Even V_f of the specimen was only 0.5%, its ϵ_f could reach 0.77%. When the specimen F2 failed, its ϵ_f reached up to 6.39%. As shown in Figure 10, ϵ_f increased significantly with the increase of V_f . Unlike ϵ_f , ϵ_c changed little when V_f increased. The relation between ϵ_c and V_f exhibited an approximate horizontal line.

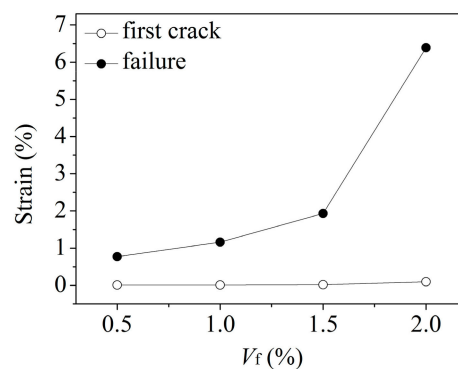


Figure 10. Influence of V_f on tensile strain.

As shown in Figure 11, both σ_c and σ_f increased clearly with the increase of V_f . But the growth of σ_f was faster than the one of σ_c . After V_f increased from 0.5% to 2%, σ_f increased by 1.68, 2.01, and 2.87 times, while σ_c increased by 1.48, 1.7, and 2.06 times. Because the small curve segment exactly represents the pullout or snap process of some PVA fibers, the more curve segments exhibits and the greater pulling capacity needs. So σ_f of the specimen F2 was the biggest. σ_f of the specimen F0.5 was the smallest.

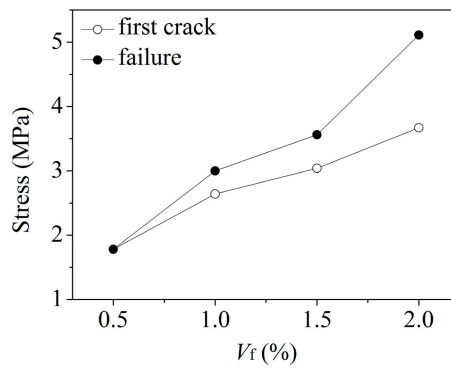


Figure 11. Influence of V_f on tensile stress.

These above results regarding the crack patterns, stress–strain curves, influence of V_f on the strain and stress of PVA-FRCM under uniaxial tension were consistent with the previous research results [12–22] which showed that remarkable tight-cracking, strain-hardening and super-high tough behaviors processed if PVA fibers were added into the matrix of cement-based composites.

4.4. Criteria on the First Crack and Failure

As mentioned above, σ_c increased significantly but ε_c changed barely with the increase of V_f . So σ_c is decisive on the first crack of specimens. After first cracking, strain and stress continue to increase until the specimen fails. The test results in Table 6 show an increasing strain growth (ε_Δ) and almost constant $\varepsilon_\Delta / \varepsilon_f$ of all specimens with the increase of PVA fiber contents. By comparison, the stress growths (σ_Δ) were less and the values of σ_Δ / σ_f of all specimens ranged from 0 to 0.28. The difference between σ_f and σ_c was small. Thus, the stress is unfit to describe the failure process of specimens, and ε_f is more appropriate.

Table 6. Strain and stress of PVA-FRCM under uniaxial tension.

V_f (%)	Strain (%)				Stress (MPa)			
	ε_c	ε_f	$\varepsilon_\Delta = \varepsilon_f - \varepsilon_c$	$\varepsilon_\Delta / \varepsilon_f$	σ_c	σ_f	$\sigma_\Delta = \sigma_f - \sigma_c$	σ_Δ / σ_f
0.5	0.01	0.77	0.76	0.99	1.78	1.78	0.00	0.00
1.0	0.01	1.16	1.15	0.99	2.64	3.00	0.36	0.12
1.5	0.02	1.93	1.91	0.99	3.04	3.56	0.52	0.15
2.0	0.09	6.39	6.30	0.99	3.67	5.11	1.44	0.28

5. Relations between Impact Resistance and Tensile Properties

5.1. Impact Failure Analysis Based on the Tensile Properties

Figure 12 shows the elements of PVA-FRCM disc specimen subjected to the dropping hammer impact. The disc specimen can be considered as many concentric circle elements (M). Each circle element (M) carries the circumferential tensile load from the impact hammer dropping. The circle element (M) can be modelled as many slab elements (N) in the radial direction and each slab element carries uniaxial tensile load. Thus, the disc specimen under the impact load can be simplified into many slabs under uniaxial tensile load in the tangential direction. Whenever the first crack appears on the slabs, it is exactly the first crack on the disc. When the strain of slab increases under the uniaxial tensile load, the crater diameter of disc specimen will also increase under the impact hammer dropping. When the slabs are pulled into pieces, the disc specimen fails.

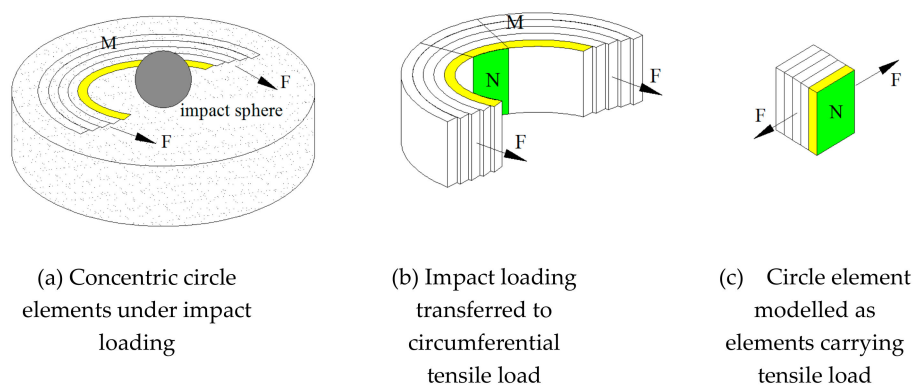


Figure 12. Elements of PVA-FRCM disc subjected to impact hammer dropping.

5.2. Relation between Blow Number N_c and Stress σ_c

Table 7 lists the major test results of the tensile properties and impact resistance. The tensile properties, σ_c and ϵ_f , and the impact resistance, blow numbers and crater diameter, are tabulated. At the first crack moment, σ_c of the slab specimen increased from 1.78 MPa to 2.64 MPa, 3.04 MPa and 3.67 MPa when more PVA fibers were added. Meanwhile, the blow number N_c of the disc specimen increased from 11 to 88, 805, and up to 1662. The relation between N_c of the disc specimen and σ_c of the slab specimen is shown in Figure 13. Although the dataset is relatively small, the general change trend can be observed that the N_c increased obviously with an increase of σ_c . The N_c of disc specimen depends largely on the σ_c of slab specimen. This phenomenon indicates that much more blows are needed to cause the appearing of first visible crack when the σ_c of PVA-FRCM is larger.

Table 7. Major test results of tensile properties and impact resistance.

V_f (%)	First Crack		Ultimate Failure		
	σ_c (MPa)	N_c	ϵ_f (%)	N_f	(mm)
0.5	1.78	11	0.77	32	29.53
1.0	2.64	88	1.16	211	35.95
1.5	3.04	805	1.93	1584	55.80
2.0	3.67	1662	6.39	3018	59.28

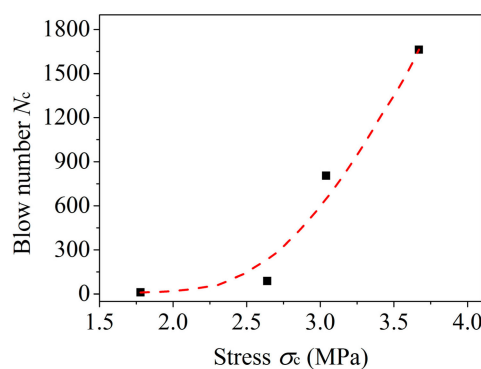


Figure 13. Relation between N_c and σ_c .

5.3. Relation between Blow Number N_f and Strain ϵ_f

Besides, it can be found that ϵ_f of the slab specimen increased from 0.77% to 1.16%, 1.93%, and 6.39% after more PVA fibers were added. The diameter of the crater in the center of disc specimen increased at the failure moment with the increase of PVA fiber content. It can be seen from Table 7, the crater diameter increased from 29.53 mm to 35.95 mm, 55.8 mm, and 59.28 mm when V_f increased. Corresponding to the crater diameter, the blow number N_f of the disc specimen increased from 32

to 211, 1548, and up to 3018. The N_f of disc specimen and ε_f of slab specimen exhibited a parabolic relationship, as shown in Figure 14. The N_f of disc specimen increased obviously with an increase of ε_f . However, this is a convex parabola which is different from the concave relation between N_c and σ_c . It might be predictable that the increase of ε_f can apparently increase N_f only within a certain range, and this effect would not be apparent exceeding that range. When the diameter of the impact crater approaches the diameter of the impact sphere, the range would be coming.

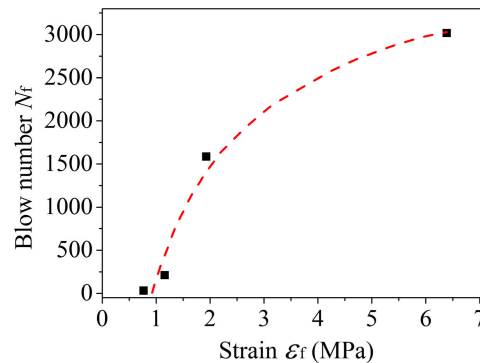


Figure 14. Relation between N_f and ε_f .

According to the presented relationships between impact resistance and tensile properties of PVA-FRCM in this study, impact resistance properties of PVA-FRCM could be conventionally evaluated or predesigned by its tensile properties without conducting extra dynamic test.

6. Conclusions

Relationships between the impact resistance and tensile properties PVA-FRCM were discussed by analyzing the experimental data of the drop-weight test and the uniaxial tension test performed in this study. The conclusions are as follows:

(1) When the disc specimen with more PVA fibers fails under the impact hammer dropping, the fibers are pulled out, the diameter of impact crater is larger, more debris appears, and more energy is consumed. The blow number increases with the PVA fiber volume content for the disc specimens. And this increase of the blow number for the ultimate failure is faster than the one for the first visible crack.

(2) In the uniaxial tension test, the slab specimen with more PVA fibers has better toughness performance and more cracks. The number of small curve segments in the tension stress–strain curves is roughly equal to the number of cracks. σ_c is decisive on the first crack of specimens. ε_f is more appropriate to describe the failure process of specimens.

(3) Based on the analysis on the relationship between the impact resistance and tensile properties, the blow number for the first visible crack N_c depends largely on σ_c of slab specimen and increases obviously with an increase of σ_c . The crater diameter and blow number at ultimate failure moment N_f increase with an increase of ε_f of slab specimen. When both σ_c and ε_f of PVA-FRCM are larger, much more blows are needed to cause both the first visible crack and ultimate failure.

(4) According to the presented relationships between impact resistance and tensile properties of PVA-FRCM in this study, impact resistance properties of PVA-FRCM could be conventionally evaluated or predesigned through its tensile properties without conducting extra dynamic test.

Author Contributions: J.Z. designed and performed the experimental work; P.B. made positive suggestions about the work; C.Y. wrote the original draft; S.L. supervised the experiments and interpreted the data; X.W. performed the experimental work.

Funding: This research was funded by the National Natural Science Foundation of China, grant numbers 51768051 and 51968056, the Inner Mongolia Natural Science Foundation, grant number 2017MS0505, and the Inner Mongolia Science and Technology Innovation Guidance Project, grant number KCBJ2018016.

Acknowledgments: The authors are grateful to Delu Zheng and Zhiwei Wang for their help in this investigation.

Conflicts of Interest: The authors declare no conflict of interest.

References

1. Rajput, A.; Iqbal, M.A. Impact behavior of plain, reinforced and prestressed concrete targets. *Mater. Des.* **2017**, *114*, 459–474. [[CrossRef](#)]
2. Gupta, T.; Sharma, R.K.; Chaudhary, S. Impact resistance of concrete containing waste rubber fiber and silica fume. *Int. J. Impact Eng.* **2015**, *83*, 76–87. [[CrossRef](#)]
3. Rahmani, T.; Kiani, B.; Shekarchi, M.; Safari, A. Statistical and experimental analysis on the behavior of fiber reinforced concretes subjected to drop weight test. *Constr. Build. Mater.* **2012**, *37*, 360–369. [[CrossRef](#)]
4. Nataraja, M.C.; Nagaraj, T.S.; Basavaraja, S.B. Reproportioning of steel fibre reinforced concrete mixes and their impact resistance. *Cem. Concr. Res.* **2005**, *35*, 2350–2359. [[CrossRef](#)]
5. Wang, H.T.; Wang, L.C. Experimental study on static and dynamic mechanical properties of steel fiber reinforced lightweight aggregate concrete. *Constr. Build. Mater.* **2013**, *38*, 1146–1151. [[CrossRef](#)]
6. Wang, L.; Wang, H.; Jia, J. Impact resistance of steel-fibre-reinforced lightweight-aggregate concrete. *Mag. Concr. Res.* **2009**, *61*, 539–547. [[CrossRef](#)]
7. Mastali, M.; Dalvand, A. The impact resistance and mechanical properties of self-compacting concrete reinforced with recycled CFRP pieces. *Compos. Part B Eng.* **2016**, *92*, 360–376. [[CrossRef](#)]
8. Mastali, M.; Dalvand, A.; Sattarifar, A.R. The impact resistance and mechanical properties of reinforced self-compacting concrete with recycled glass fibre reinforced polymers. *J. Clean. Prod.* **2016**, *124*, 312–324. [[CrossRef](#)]
9. Kim, M.J.; Kim, S.; Lee, S.K.; Kim, J.H.; Lee, K.; Yoo, D.Y. Mechanical properties of ultra-high-performance fiber-reinforced concrete at cryogenic temperatures. *Constr. Build. Mater.* **2017**, *157*, 498–508. [[CrossRef](#)]
10. Li, Z.X.; Li, C.H.; Shi, Y.D.; Zhou, X.J. Experimental investigation on mechanical properties of Hybrid Fibre Reinforced Concrete. *Constr. Build. Mater.* **2017**, *157*, 930–942. [[CrossRef](#)]
11. Sorelli, L.G.; Meda, A.; Plizzari, G.A. Bending and uniaxial tensile tests on concrete reinforced with hybrid steel fibers. *J. Mater. Civ. Eng.* **2005**, *17*, 519–527. [[CrossRef](#)]
12. Zhang, Y.H.; Zhang, Z.P.; Liu, Z.C. Graphite coated PVA fibers as the reinforcement for cementitious composites. *Mater. Res. Express.* **2018**, *5*, 025206. [[CrossRef](#)]
13. Li, V.C.; Wang, S.X.; Wu, C. Tensile strain-hardening behavior of polyvinyl alcohol engineered cementitious composite (PVA-ECC). *ACI Mater. J.* **2001**, *98*, 483–492.
14. Li, V.C.; Wu, C.; Wang, S.X.; Ogawa, A.; Saito, T. Interface tailoring for strain-hardening polyvinyl alcohol engineered cementitious composite (PVA-ECC). *ACI Mater. J.* **2002**, *99*, 463–472.
15. Nematollahi, B.; Sanjayan, J.; Shaikh, F.U.A. Tensile strain hardening behavior of PVA fiber-reinforced engineered geopolymer composite. *J. Mater. Civ. Eng.* **2015**, *27*, 04015001. [[CrossRef](#)]
16. Li, H.D.; Xu, S.L.; Leung, C.K.Y. Tensile and flexural properties of ultra high toughness cementitious composite. *J. Wuhan Univ. Technol. Mater. Sci. Ed.* **2009**, *24*, 483–492. [[CrossRef](#)]
17. Yang, E.H.; Li, V.C. Tailoring engineered cementitious composites for impact resistance. *Cem. Concr. Res.* **2012**, *42*, 1066–1071. [[CrossRef](#)]
18. Toutanji, H.; Xu, B.; Gilbert, J.; Lavin, T. Properties of poly(vinyl alcohol) fiber reinforced high-performance organic aggregate cementitious material: Converting brittle to plastic. *Constr. Build. Mater.* **2010**, *24*, 1–10. [[CrossRef](#)]
19. Xu, B.; Toutanji, H.A.; Gilbert, J. Impact resistance of poly(vinyl alcohol) fiber reinforced high-performance organic aggregate cementitious material. *Cem. Concr. Res.* **2010**, *40*, 347–351. [[CrossRef](#)]
20. Mechtcherine, V.; Millon, O.; Butler, M.; Thoma, K. Mechanical behaviour of strain hardening cement-based composites under impact loading. *Cem. Concr. Compos.* **2011**, *33*, 1–11. [[CrossRef](#)]
21. Curosu, I.; Mechtcherine, V.; Millon, O. Effect of fiber properties and matrix composition on the tensile behavior of strain-hardening cement-based composites (SHCCs) subject to impact loading. *Cem. Concr. Res.* **2016**, *82*, 23–35. [[CrossRef](#)]
22. Atahan, H.N.; Pekmezci, B.Y.; Tuncel, E.Y. Behavior of PVA fiber-reinforced cementitious composites under static and impact flexural effects. *J. Mater. Civ. Eng.* **2013**, *25*, 1438–1445. [[CrossRef](#)]

23. Batista, R.P.; Trindade, A.C.C.; Borges, P.H.R.; Silva, F.D. Silica Fume as Precursor in the Development of Sustainable and High-Performance MK-Based Alkali-Activated Materials Reinforced with Short PVA Fibers. *Front. Mater.* **2019**, *6*. [[CrossRef](#)]
24. Arain, M.F.; Wang, M.X.; Chen, J.Y.; Zhang, H.P. Study on PVA fiber surface modification for strain-hardening cementitious composites (PVA-SHCC). *Constr. Build. Mater.* **2019**, *197*, 107–116. [[CrossRef](#)]
25. Du, Q.; Wei, J.; Lv, J. Effects of High Temperature on Mechanical Properties of Polyvinyl Alcohol Engineered Cementitious Composites (PVA-ECC). *Int. J. Civ. Eng.* **2018**, *16*, 965–972. [[CrossRef](#)]
26. Bao, W.B.; Wang, C.H.; Zhang, S.F.; Huang, Z.Q. Experimental study on mechanical properties of PVA fiber reinforced tailings cementitious composites. *Architect. Urb. Develop.* **2012**, *598*, 618–621. [[CrossRef](#)]
27. Salami, B.A.; Johari, M.A.M.; Ahmad, Z.A.; Maslehuddin, M. Durability performance of Palm Oil Fuel Ash-based Engineered Alkaline-Activated Cementitious Composite (POFA-EACC) mortar in sulfate environment. *Constr. Build. Mater.* **2017**, *131*, 229–244. [[CrossRef](#)]
28. Sherir, M.A.A.; Hossain, K.M.A.; Lachemi, M. Fresh state, mechanical & durability properties of strain hardening cementitious composite produced with locally available aggregates and high volume of fly ash. *Constr. Build. Mater.* **2018**, *189*, 253–264. [[CrossRef](#)]
29. Baral, K.; Tatar, J.; Zhang, Q. High-Performance Impact-Resistant Concrete Mixture for Transportation Infrastructure Applications. *Transp. Res. Rec.* **2019**. [[CrossRef](#)]
30. Halvaei, M.; Jamshidi, M.; Latifi, M.; Behdooj, Z. Application of Low Modulus Polymeric Fibers as Reinforcement in Engineered Cementitious Composite (ECC). In Proceedings of the 7th Asian Symposium on Polymers in Concrete, Istanbul, Turkey, 3–5 October 2012; pp. 787–794.



© 2019 by the authors. Licensee MDPI, Basel, Switzerland. This article is an open access article distributed under the terms and conditions of the Creative Commons Attribution (CC BY) license (<http://creativecommons.org/licenses/by/4.0/>).